Monitoring of Thermal Energy Distribution in Abrasive Waterjet Cutting Using Infrared Thermography

R. Kovacevic

R. Mohan*

H. E. Beardsley

Center for Robotics and Manufacturing Systems and Department of Mechanical Engineering, University of Kentucky, Lexington, KY

Thermal energy distribution in the workpiece cut with abrasive waterjet (AWJ) is analyzed using the technique of infrared thermography through isotherms and line-scans. Variation in workpiece temperature with thermal conductivity and cutting conditions is studied. The feasibility of visualization of AWJ cutting mechanisms in opaque materials using infrared thermography is investigated. A novel technique of AWJ nozzle wear monitoring through infrared thermography is proposed. A comparative study of infrared thermography results with the readings of thermocouples and the two-dimensional moving line heat source model show a close correspondence indicating that infrared thermography is a good technique for the above application.

1 Introduction

As a new manufacturing process, abrasive waterjet (AWJ) cutting has been very effective in machining difficult-to-machine materials. This cutting technique is one of the most recently introduced machining methods in which an abrasive such as garnet, aluminum oxide or silicon carbide is accelerated by a thin stream of high velocity waterjet and directed through an AWJ nozzle towards the target material. Contrary to the traditional manufacturing processes, the absence of thermal effects and heat affected zone in this process have tempted us to often refer to this technique as a cold-jet cutting process.

Being an erosion process, here the workpiece is heated only by about 50°C more than the atmospheric temperature. However, cutting of materials like titanium yields spark showers and water vapor at the cutting zone indicating the existence of highly localized heating effects. Thermal sensitive materials like certain poly-carbonates, plastics, glass, certain composite materials and bio-materials like bones are subjected to structural deformation and crack formation when exposed to temperature rise of even a few degrees. Due to its localized heating effects the AWJ stream can be considered as a moving heat source. Therefore, there is a need to investigate the source of heat generation and its distribution in the workpiece as well as the abrasive waterjet nozzle.

Presently, there is a very limited knowledge about the generated heat and thermal energy distribution through the workpiece during cutting with AWJ. There has been only one systematic study of the thermal energy distribution in the workpiece during cutting with AWJ. Ohadi et al. [1, 2] monitored the workpiece temperature using thermocouples embedded at different points in the workpiece through previously drilled holes. However, this method has the inherent limitation that the workpiece preparation for experiments is tedious. Also, this method gives the temperature variation at previously selected points only.

The main objective of the current study is to use infrared (IR) thermography for the evaluation of the thermal energy distribution in the workpiece and AWJ nozzle during cutting under different conditions. The feasibility of using this technique to visualize the erosion mechanism of AWJ in opaque materials and monitoring the nozzle wear are also investigated. Two different workpiece materials (aluminum and titanium) of different thermal conductivities are used for this purpose. Temperature measurements are taken using thermocouples at different locations in the plane parallel to the cut surface to verify the accuracy of the infrared thermography results. The IR results are also compared with theoretical analysis using a two dimensional moving line heat source model.

Infrared video cameras are used extensively in nonmanufacturing areas like night vision, surveillance, targeting and identification, foul weather and night-landing aids, leak detection, stress pattern recognition, oil pollution control, fire fighting, meteorological studies, land surveys, medical analysis etc. [3]. Infrared thermography has been used as a sensing technique for temperature measurements in various manufacturing processes also. It is used for visualizing heat flow in fluids, controlling laser machining, monitoring and controlling laser welding [4], arc welding [5–6], fusion welding [7], measurement of temperature generated during grinding of materials like ceramics, [8] etc. Infrared thermographic inspection is used [9] for evaluating bonded composite honeycomb structures that are difficult or impossible to evaluate using conventional ultrasonics.

Hashish [10] has conducted extensive investigations using high-speed cameras to visualize the AWJ cutting process in transparent materials like Lexan, Lucite and glass. Even though this method is very useful to study the AWJ cutting process in transparent materials, it cannot be adopted for opaque materials. Infrared thermography is a very promising technique for obtaining more information about the various mechanisms involved in cutting opaque materials by abrasive waterjet.

The AWJ nozzle is one of the most critical parts that influences the technical and economical performance of an AWJ cutting system. Direct and indirect methods have been used for monitoring the AWJ nozzle wear. Direct sensing techniques [11] have the disadvantage that they cannot be successfully used for monitoring a continuous increase in AWJ nozzle inner diameter (ID) without interrupting the cutting process. The indirect methods are promising approaches for on-line sensing of the nozzle wear and compensating for the increase in nozzle inside diameter. These methods are based on the measurement of parameters that are correlated to the AWJ nozzle wear such as the change in the stream diameter at the nozzle exit [12], or the change in workpiece normal force generated by the im-

* Present Address: Department of Mechanical Engineering, The University of Tulsa, Tulsa, OK.

Contributed by the Manufacturing Engineering Division for publication in the JOURNAL OF MANUFACTURING SCIENCE AND ENGINEERING. Manuscript received Sept. 1994; revised July 1995. Associate Technical Editor: K. Rajurkar.

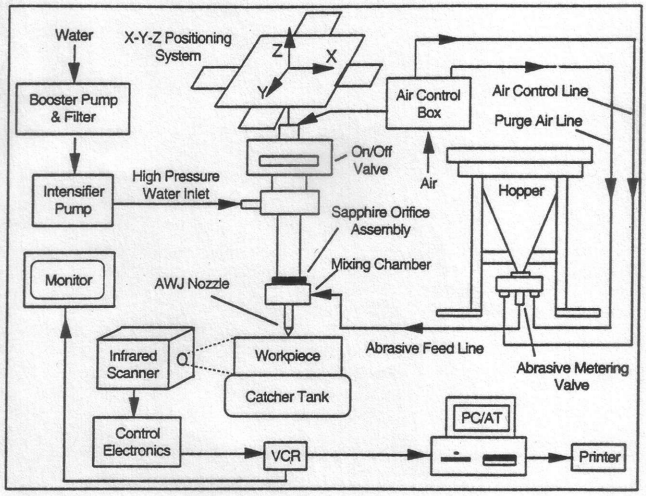

Fig. 1 Schematic of experimental setup

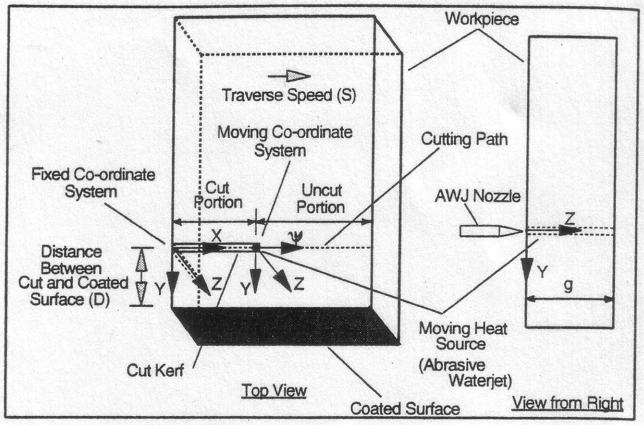

Fig. 2 Workpiece/jet co-ordinate system

pacting jet [13], or through acoustic signature analysis [14]. However, there has not been any attempt to measure the AWJ nozzle temperature and monitor the nozzle wear through temperature sensing.

The objective of this investigation is to use the technique of infrared thermography to monitor the following:

- Thermal energy distribution in workpiece cut with AWJ with change in cutting conditions and workpiece material. Use this information to determine the heat flux at the cutting zone.
- Visualization of the AWJ cutting mechanisms in opaque materials.
- Temperature distribution in AWJ cutting nozzle and thereby indirectly monitor the nozzle wear.
- Quantitative comparisons of the infrared thermography results with those obtained using thermocouples and the moving line heat source model.

2 Experimental Set-up

The experimental set-up consists of an abrasive waterjet cutting system, an infrared system, a video cassette recorder, a PC/AT with custom-developed software for thermo-image processing and the workpiece. The abrasive waterjet cutting system used for conducting the experiment includes a high pressure intensifier pump, abrasive metering and delivery system, AWJ cutting head, catcher tank, and an X-Y-Z positioning table controlled by a CNC controller. The infrared system includes the infrared scanner, control electronics, and monitor. A schematic of the experimental set-up is shown in Fig. 1. Two different types of materials, Al 2024 and Ti-alloy (R58640; Ti-3Al-8V-6Cr-4Mo-4Zr; also called 'Beta C') of different thermal conductivities (see Table 1) are chosen for investigation. The process parameters chosen for evaluation are water pressure, traverse speed, and distance between cut and coated surface (Fig. 2).

This experiment is conducted in three phases. The first phase focuses on the influence of the above parameters on the temperature distribution in the aluminum workpiece. The process parameters for phase I are given in Table 2. The second phase is conducted to investigate the influence of the workpiece thermal conductivity on the pattern of temperature distribution for the two selected materials. Process parameters for this phase are given in Table 3. Detailed analysis of the temperature distribution on both workpieces is conducted to visualize the striation generating mechanism by abrasive waterjet at various stages of cutting. The images produced from the IR data of the opaque materials are used for comparison with the results of the visualization studies conducted previously [10] for transparent materials. Temperature measurements are taken using thermocouples

Table 1 Workpiece properties

Property	Aluminum	Ti-alloy
Thermal Conductivity (K)	177 $W/m°K$	6.54 $W/m°K$
Volumetric Heat Capacity (ρC_p)	2.424 $MJ/m^3°K$	2.482 $MJ/m^3°K$
Thermal Diffusivity (α)	73.0 X $10^{-6} m^2$/sec	2.64 X $10^{-6} m^2$/sec
Nusselt Number (N_L)*	8.5319	8.5319
Grashof's Number (Gr_L)*	7.2638 X 10^4	7.2638 X 10^4
Prandtl Number (Pr)*	0.7100	0.7100
Convective Heat Transfer Coeff. (h)	8.5319 $W/m^2°K$	8.5319 $W/m^2°K$
Radiative Heat Transfer Coeff. (h_r)*	6.9132 $W/m^2°K$	6.9132 $W/m^2°K$
Biot Number (B_i)	1.29 X 10^{-3}	3.49 X 10^{-2}

* - these parameters calculated for T_0 of 293°K and T_s of 333°K

Table 2 Influence of AWJ process parameters (phase I)

Workpiece Details		Experimental Variables			
Material	- Al 2024	Trial No.	Water Pressure(P) (MPa)	Traverse Speed(S) (mm/s)	Distance (D) of Coated Surface (mm)
Material Thickness	- 25.4 mm				
Length of cut	- 46.0 mm				
Constant Parameters		1	241	1.06	2.54
		2	276	1.06	2.54
AWJ orifice material	- Sapphire	3	310	1.06	2.54
AWJ orifice diameter	- 0.254 mm	4	276	0.85	5.08
Mixing nozzle Length	- 76.2 mm	5	276	1.06	5.08
Mixing nozzle diameter	- 0.762 mm	6	276	1.27	5.08
Method of feed	- suction	7	310	1.06	10.16
Angle of Jet	- 90°	8	310	1.06	17.78
Abrasive material	- Garnet	9	310	1.06	25.40
Abrasive mesh size	- 80 (0.180 mm)				
Abrasive particle shape	- angular(random)				
Condition of abrasive	- dry				
Abrasive Flow Rate	- 5.3 g/s				
Stand-off Distance	- 4.00 mm				

Table 3 Workpiece conductivity (phase II)

Constant Parameters			
AWJ orifice material	- Sapphire	AWJ orifice diameter	- 0.254 mm
Mixing nozzle length	- 76.2 mm	Mixing nozzle dia.	- 0.762 mm
Method of feed	- suction	Angle of Jet	- 90°

Variable Parameters	Aluminum (Al 2024)	Ti alloy (R58640)
Abrasive material	- Garnet	- Aluminum Oxide
Abrasive mesh size	- 80 (0.180 mm)	- 100 (0.144 mm)
Abrasive particle shape	- angular(random)	- angular(random)
Condition of abrasive	- dry	- dry
Abrasive Flow Rate	- 5.3 g/s	- 6.05 g/s
Water Pressure (P)	- 310 MPa	- 310 MPa
Traverse Speed (S)	- 1.06 mm/s	- 0.51 mm/s
Stand-off Distance	- 4.00 mm	- 4.00 mm
Material thickness	- 25.4 mm	- 25.4 mm
Length of cut	- 46.0 mm	- 35.0 mm
Distance of Coated Surface (D)	- 2.54 mm, 10.16 mm, 17.78 mm & 25.4 mm	- 2.54 mm, 3.18 mm, & 9.53 mm

Table 4 Nozzle wear (phase III)

Constant Parameters	
AWJ orifice material	- Sapphire
AWJ orifice diameter	- 0.254 mm
Mixing nozzle length	- 76.2 mm
Method of feed	- suction
Angle of Jet	- 90 degrees
Abrasive material	- Garnet
Abrasive mesh size	- 80 (0.180 mm)
Abrasive particle shape	- angular(random)
Condition of abrasive	- dry
Abrasive Flow Rate	- 5.3 g/s
Water Pressure (P)	- 262 MPa
Experimental Variable	
Nozzle Inner Diameter	- 1.02 mm, 1.40 mm, and 1.63 mm

at different locations in the plane parallel to the cut surface to verify the IR thermography results. The analysis of the influence of nozzle wear on the temperature distribution in the AWJ nozzle is conducted in the phase III. Isotherms are plotted for various nozzle ID's keeping the other parameters constant. The process parameters for this phase are given in Table 4.

When infrared radiation from a surface is to be measured, the emissivity of that surface must be known and it should remain constant throughout the measurement period. Therefore, for the above experiments, the test surfaces were coated with black enamel of emissivity 0.99. Figure 2 gives a schematic of the workpiece details. The infrared radiation emitted from such prepared surfaces which characterizes the thermal energy distribution is detected by an infrared camera (Inframetrics, model 600). The IR images were recorded on video tape for further analysis. Each scan of the camera is transferred as a frame consisting of 170 × 170 discrete gray level values which are converted to temperatures (°C). Thermocouples (K-Type, omega-alumega, 0.07 mm diameter) were attached at various locations on the coated surfaces of the workpiece using epoxy for phase II experiments. Voltage is measured by the thermocouples and converted into absolute temperatures using the National Bureau of Standards voltage conversion coefficients.

3 Theoretical Analysis

The workpiece temperature distribution during cutting with AWJ was obtained using thermocouples by Ohadi and Cheng [2] and the two-dimensional moving line heat source model developed by Rosenthal [15] was adopted for comparison. As the heat flux, q could not be determined directly (due to the complexity of the problem), an inverse heat conduction (IHC) method proposed by Beck and Arnold [16] was utilized for this purpose. In this paper, the results obtained using infrared thermography are compared with the analytical approach followed on similar lines. A brief description about the direct heat conduction problem and inverse heat conduction problem are given below.

3.1 Direct Heat Conduction Problem. The convective heat transfer coefficient, h determined for the given experimental conditions for both workpiece materials using the corresponding Nusselt number, Grashof's number and Prandtl number are shown in Table 1. The radiative heat transfer coefficient, h_r, which is a function of temperature, is determined using the standard equation,

$$h_r = \epsilon\sigma(T_s + T_0)(T_s^2 + T_0^2) \tag{1}$$

where, ϵ is the emissivity of the surface and σ is the Stefan-Boltzmann constant. The values of h_r corresponding to a typical T_0 of 20°C and T_s of 60°C are also given in Table 1. As $h = O(h_r)$, it can be concluded that the convective and radiative components of heat transfer are of equivalent magnitudes. The Biot number, B_i (also shown in the above table) is given by,

$$B_i = \frac{hg}{K} \tag{2}$$

where, g is the characteristic length (thickness of the workpiece) and K is the thermal conductivity of the solid. B_i of aluminum is of the $O(10^{-3}) \ll 1.0$ and titanium is of the $O(10^{-2}) \ll 1.0$. From this, it can be concluded that the resistance to conduction within the solid for both materials is much less than resistance to convection across the fluid(air)/solid boundary layer. Thus the heat loss due to convection and radiation can be ignored for modeling as their magnitudes are much less than that of conduction. Assuming negligible heat loss, the differential equation of heat flow for an isotropic homogeneous material in rectangular co-ordinates with fixed origin in the solid, has the form,

$$\frac{\partial^2 T}{\partial x^2} + \frac{\partial^2 T}{\partial y^2} + \frac{\partial^2 T}{\partial z^2} = 2\lambda \frac{\partial T}{\partial t} \tag{3}$$

where, x, y, and z are the co-ordinate axes with fixed origin (Fig. 2), T is the temperature, t is the time and $2\lambda = c\rho/K$ if c is the specific heat and ρ is the density. Assuming the workpiece to be long enough so that quasi-stationary condition is reached, the general 3-dimensional heat flow equation for line heat source moving at a constant speed, S can be derived from (2) and is given [15] as,

$$\frac{\partial^2 T}{\partial \psi^2} + \frac{\partial^2 T}{\partial y^2} + \frac{\partial^2 T}{\partial z^2} = -2\lambda S \frac{\partial T}{\partial \psi} \tag{4}$$

where, ψ, y, and z are the co-ordinate axes with the line source as origin.

Due to the linear nature of the heat source (in this case, AWJ) the temperature gradient in the Z-direction is very small and hence the heat flow in that direction can be ignored. Thus the solution of equation (4) in the two-dimensional case assuming a line source of heat is given [15] as,

$$T - T_0 = \frac{q}{2\pi Kg} e^{-\lambda S\psi} K_0(\lambda S r) \tag{5}$$

where, T_0 is the initial temperature of the workpiece, q is the heat flux, $K_0(\lambda Sr)$ is the modified Bessel function of the second kind with zero order and r is given by, $r = \sqrt{\psi^2 + y^2}$. The boundary conditions adopted for the above solution are,

$$\frac{\partial T}{\partial \psi} \to 0 \quad \text{as} \quad \psi \to \pm\infty$$

$$\frac{\partial T}{\partial y} \to 0 \quad \text{as} \quad y \to \pm\infty \tag{6}$$

It may be noted that, at the cut portion (Fig. 2), the workpiece width is small and hence there is a subsequent rise in the initial temperature of the plate followed by a slow cooling [17]. Therefore it takes more time to reach quasi-stationary condition. Whereas, the uncut region reaches steady-state condition almost instantaneously due to the presence of the bulk material. Thus, as there is a negligible heat loss through the surface, additional boundary condition to be satisfied for the cut portion is

$$\frac{\partial T}{\partial y} = 0 \quad \text{for} \quad y = +D \tag{7}$$

Using the mirror method suggested by Rosenthal [17], the additional boundary condition defined by Eq. (7) can be applied to Eq. (5). The resulting equation for temperature distribution is

$$T - T_0 = \frac{q}{\pi Kg} e^{-\lambda S\psi} K_0(\lambda S r) \tag{8}$$

Equation (5) is used for the condition, $\psi > 0$ and equation (8) is used when $\psi < 0$.

3.2 Inverse Heat Conduction Problem. The heat flux to the workpiece at various cutting conditions were determined through inverse heat conduction method. A parameter estimation approach proposed by Beck and Arnold [16] which uses the experimentally determined temperature histories at various points in the workpiece, was adopted for this calculation. These points were chosen along a horizontal line passing through the middle of the coated surface at a distance of 2.5 mm from the kerf for better accuracy of the estimation. Two points were chosen close to the entry zone, two close to the exit zone and four points equally spaced at the middle of the workpiece. The least squares error, E between the computed temperature, $T_c(i, j, q)$ and the measured temperature, $T_m(i, j)$ for p (= 8, here) locations and n future time steps is given by,

$$E = \sum_{i=1}^{p} \sum_{j=1}^{n} [T_m(i,j) - T_c(i,j,q)]^2$$
$$= \sum_{i=1}^{p} \sum_{j=1}^{n} [T_m(i,j) - (T_0 + qG(i,j))]^2 \quad (9)$$

as $T_c(i, j, q)$ is given by,

$$T_c(i,j,q) = T_0 + qG(i,j)$$

where, the sensitivity coefficient,

$$G(i,j) = \frac{\partial T_c(i,j,q)}{\partial q}$$

which can be obtained from Eq. (5) or Eq. (8) based on the instantaneous location of the point under consideration with respect to the heat source.

In order to minimize the least square error, E, Eq. (9) is to be differentiated with respect to q and equated to zero which gives,

$$\frac{\partial E}{\partial q} = \sum_{i=1}^{p} \sum_{j=1}^{n} [T_m(i,j) - T_c(i,j,q)](-2G(i,j)) = 0 \quad (10)$$

Taylor Series expansion about an arbitrary heat flux, $\tilde{q}$ gives,

$$T_c(i,j,q) = T_c(i,j,\tilde{q}) + (q - \tilde{q})G(i,j)) \quad (11)$$

As $T_c(i, j, q)$ is a linear function of q, the second and higher order derivatives in Eq. (11) are zero. Substituting Eq. (11) in Eq. (10) and replacing q by $\hat{q}$ (estimator of q) in the resulting equation, gives after simplification

$$\sum_{i=1}^{p} \sum_{j=1}^{n} [T_m(i,j) - (T_0 + \tilde{q}G(i,j))]G(i,j)$$
$$- \{(\hat{q} - \tilde{q}) \sum_{i=1}^{p} \sum_{j=1}^{n} G(i,j)^2\} = 0 \quad (12)$$

Thus,

$$\hat{q} = \tilde{q} + \frac{\sum_{i=1}^{p} \sum_{j=1}^{n} [T_m(i,j) - (T_0 + \tilde{q}G(i,j))]G(i,j)}{\sum_{i=1}^{p} \sum_{j=1}^{n} G(i,j)^2} \quad (13)$$

Thus the estimated value of the heat flux, $\hat{q}$ is used in Eq. (5) and Eq. (8) to obtain the analytical temperature distribution.

4 Results and Discussion

The discrete temperatures calculated from the gray level values are processed further to obtain the pattern of temperature distribution on the coated surfaces. Two different representational methods, namely isotherms and linescans are used for the analysis of the IR data. Isotherms are the loci of points of equivalent temperatures, whereas linescans are thermal profiles along selected lines. Isotherms and linescans are obtained from an IR image frame which represents a particular instant when the abrasive waterjet nozzle has passed one half of the length of cut. Temperatures along the horizontal line passing across the middle of the coated surface are used to plot the linescan. Water pressure (P), traverse speed (S), and distance between the coated and cut surface (D) were varied in order to analyze their influence on the generated thermal energy during AWJ cutting of aluminum. Each parameter was varied while keeping the other two constant to investigate its independent influence on the temperature distribution in the workpiece.

4.1 Water Pressure. The linescans along the middle of the coated surface with change in water pressure are plotted in Fig. 3(*a*). These linescans indicate that with increase in water pressure the workpiece temperature increases. The trend in the temperature distribution can be attributed to the following. As water pressure increases, the jet velocity also increases and in turn increases the workpiece normal force. This results in higher frictional forces at the jet-workpiece interface in the cutting zone and consequently the overall temperature of the workpiece increases. Through the inverse heat conduction problem described in section 3.2, the rate of heat input to the workpiece for different water pressures is determined. The variation of estimated heat flux with change in water pressure is plotted in Fig. 4(*a*). From this figure it can be noted that with increase in water pressure the heat flux at the kerf increases linearly which causes the workpiece temperature to increase.

During cutting, the portion of the workpiece ahead of the jet is in physical contact with the bulk of the material which is being cut, whereas the portion of the workpiece behind the jet (cut portion) is not. As the heat source has not reached the uncut portion, and since it takes time for the heat to be conducted to that region, its temperature does not rise as high or as fast as the cut portion which has already been in contact with the heat source and the energy from the source has already been conducted into that region. Hence the uncut portion is relatively cooler than the cut portion.

Using the two-dimensional moving line heat source model described in section 3, temperature distribution along the horizontal line through the middle of the coated surface is plotted for various water pressures in Fig. 5(*a*) as typical examples for comparison with the experimental data. It may be noted that the model and the experimental data have a very close correlation with an RMS error < 1.5°C indicating that the heat flux estimate is fairly accurate. A point on the above horizontal line which is about 22 mm from the left edge of the workpiece is chosen to plot the time-temperature graph shown in Fig. 5(*b*). It can be seen from this time domain graph that the model and the IR results match very closely as the heat source approaches the point of observation and after it leaves. The predicted temperature of the model is higher than the IR thermography results when the heat source is farther behind the point of observation. This is because the workpiece has a finite length along the ψ direction whereas the model was derived for the general case of a workpiece of infinite length. However, as the primary objective of a thermal analysis of the workpiece in AWJ cutting is to predict/measure the maximum temperature at the cutting zone so as to avoid material failure, this discrepancy can be ignored. Above analysis indicates that the infrared sensing method gives reliable results at various cutting conditions.

4.2 Traverse Speed. The linescans for different traverse speeds are shown in Fig. 3(*b*). With the increase in speed there is only a marginal increase in peak temperatures. The same trend is reflected in the heat flux graph shown in Fig. 4(*b*). This indicates that change in traverse speed does not have a considerable influence on the estimated heat flux or the temperature distribution pattern in the workpiece. As in the case of

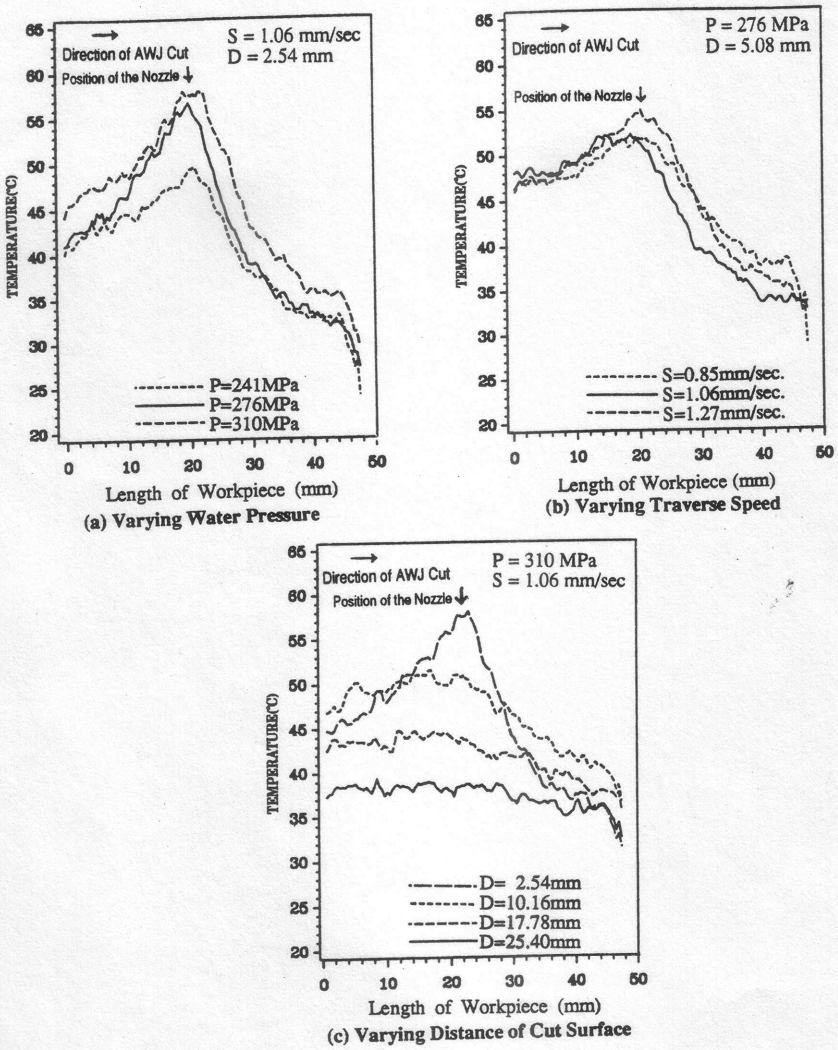

Fig. 3 Linescans for phase I (aluminum)

varying water pressures, here also it is evident (from the linescan graph) that the cut portion of the workpiece is hotter than the uncut portion. As the kinetic energy of the waterjet remains the same for constant water pressure and constant abrasive flow rate, the heat input and in turn heat flux should be constant. The marginal increase in the heat flux with increase in traverse speed can be attributed to the assumptions adopted for the analytical model namely negligible heat loss, linear heat source, isotropic homogeneous material, assumption of two-dimensional heat flow, idealized boundary conditions and quasi-steady state condition of the workpiece material and the experimental errors in the temperature readings. However, as the increase in heat flux is not significant, it can be ignored.

4.3 Distance from Cutting Plane. Linescans along the middle of the coated surface which are at different distances from the cut kerf are plotted in Fig. 3(*c*). These linescans indicate that higher temperatures are present on the planes closer to the cutting zone. As mentioned previously, the AWJ can be considered as a moving heat source. This heat source increases the temperature of the narrow zone along the kerf wall. The temperature gradient on the plane closest to the jet is steep, indicating the locally concentrated heating along the kerf wall. However, for the planes farther from the jet axis the temperature gradients have been smoothed by heat conduction through the material closer to the cut. Similar to the previous two cases, the reasons mentioned in section 4.1 are responsible for higher temperature of the cut portion of the workpiece.

4.4 Thermal Conductivity. It is expected that a change in thermal conductivity of the material will yield a different temperature distribution pattern in the workpiece. Hence workpieces of similar heat capacities and contrasting thermal conductivities (Al 2024 as a good conductor of heat and Ti-alloy (R58640) as a poor conductor of heat) are used here for investigation.

The influence of the difference in thermal conductivities of the above materials can be easily understood if we compare temperature distribution patterns on vertical planes which are placed at the same distance from the cut kerf. Figure 6(*b*) gives the isotherms for aluminum at a distance of 2.5 mm from the cut kerf and Fig. 7(*b*) gives the isotherms for titanium at a distance of 2.5 mm from the cut kerf when the nozzle has traversed approximately half the length of cut. It may be noted that, in the case of titanium, two peak temperatures are present, one in the upper half and one in the lower half indicating the presence of two different wear modes namely cutting wear mode and deformation wear mode. On the contrary, even though both wear modes are existing in aluminum only one peak temperature is observed which is at the point when deformation wear starts. This could be due to the presence of weaker striations (or better surface finish) compared to that of the titanium. These modes are discussed in detail in section 4.5. It was observed that for titanium, the isotherms even for the plane at a distance of 10 mm from the kerf are capable of revealing the jet flow pattern and in turn providing information about the striation angle.

Whereas in the case of aluminum the jet flow pattern was clear only in the plane close (2.5 mm away) to the kerf. This can be attributed to their respective thermal diffusivities. Even though their heat capacities are same (of the $O(2.4\ \mathrm{MJ/m^3°K})$), the thermal diffusivity of aluminum is much higher than that of titanium (see Table 1). Hence titanium will respond more sluggishly to changes in its thermal environment taking longer time to reach a new equilibrium condition. Thus infrared imaging can provide more information related to the AWJ cutting mechanisms in terms of jet flow pattern and wear modes for materials having lower thermal diffusivity.

The linescans for the three titanium cuts which are at different distances from the coated surface are shown in Fig. 8. Behavior of the peak temperatures is similar to that of the peak points in the isotherms. Titanium being a poor conductor of heat, a longer time is needed for heat to penetrate out to the measured surface. This is the reason that, though the jet is in the same position for all three cuts, the peak temperatures are displaced (with respect to the jet direction) with increase in distance of the measured surface. Contrary to the linescans obtained for aluminum, the temperature of the cut and uncut portions of the titanium workpiece are approximately the same due to its low thermal conductivity.

4.5 Visualization of AWJ Cutting Mechanisms in Opaque Materials. Even though a detailed investigation was done on visualization of the AWJ cutting process in transparent materials through high speed photography [10], there has not been a similar study for opaque materials. Infrared thermography gives us an opportunity to conduct visualization studies on opaque materials.

A typical AWJ cut surface is characterized by two distinctly different regions. The upper region, known as the cutting wear zone [10, 18] is relatively smooth and devoid of any striation marks. The surface finish of this zone is comparable with that

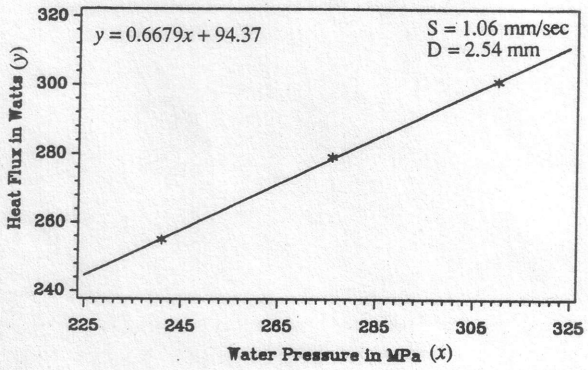

(a) Varying Water Pressure

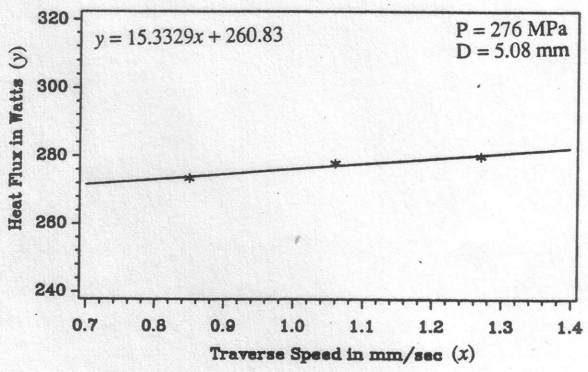

(b) Varying Traverse Speed

Fig. 4 Heat flux vs. process parameters (phase I)

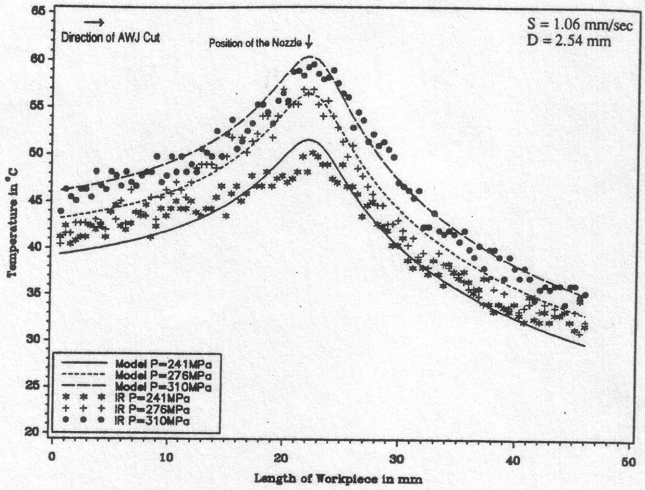

Fig. 5(*a*) Comparison of model and infrared results–space domain (aluminum)

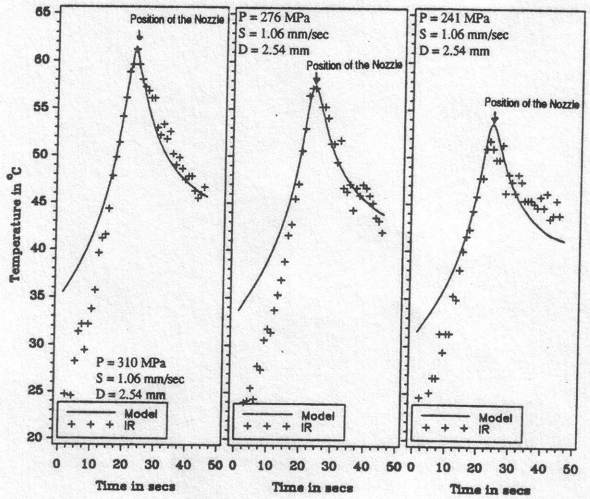

Fig. 5(*b*) Comparison of model and infrared results–time domain (aluminum)

of surfaces produced with finishing operations, such as grinding [18]. Previous observations indicate that as we move downwards along the kerf wall, striations begin to appear. The bottom region where the striations are present is called the deformation wear zone [10]. In this region the presence of the striations predominantly dictate the surface quality. In AWJ cutting, the mechanisms responsible for machining, namely micro-machining, shearing and erosion, result in negligible amounts of induced surface strain. As the high velocity waterjet mixed with abrasive penetrates into the workpiece, it loses its kinetic energy gradually as it moves along the kerf wall, and as a result the jet starts deflecting away from its axis. In the cutting wear zone the material removal occurs primarily due to particle impact at shallow angles. In this case the particle impacts the material, plows a trajectory, and exits [10]; whereas in the deformation wear zone the particles impact at large angles and the mode of erosion is characterized by excessive deformation which results in work hardening and chipping of the material. The striations on the titanium surface start appearing approximately at the middle of the kerf wall. On the other hand, for the aluminum cut surface, striations start appearing after the jet has penetrated almost three fourths of the kerf wall. Moreover the striation angles are greater in the case of titanium than aluminum. Both these phenomena can be attributed to the difference in mechanical properties of materials, i.e. hardness and brittleness, the abrasives used and the abrasive flow rate.

The temperature distribution on the workpiece surfaces for three different instances of the jet position, namely entry stage (when jet starts cutting), cutting stage (when jet has traversed approximately half the length of cut), and exit stage (when jet leaves the workpiece) are plotted in Fig. 6 and Fig. 7 for aluminum and titanium respectively. As observed earlier, the isotherms follow the jet flow pattern in the workpiece. Thus, information regarding the behavior of the jet during the cutting process can be retrieved through the pattern of the isotherms. The inclination of the isotherms correspond to the striation marks observed on the surfaces. The isotherms of the titanium workpiece have a larger inclination than those of the aluminum workpiece. This can be directly related to the difference in the striation angle of these two workpieces. It can be observed from Fig. 6 and Fig. 7 that, as the cut progresses, the average workpiece temperature gradually increases. This steady increase in the peak temperatures of the workpiece from entry stage to exit stage is because of heat conduction from the cut portion to the uncut portion. One of the peak temperatures observed in the titanium workpiece is at the middle of the cutting wear zone, and the other is at the middle of the deformation wear zone, indicating the existence of a relatively colder region in the transition zone. The effect of the uncut triangle at the exit edge of the workpiece is depicted by a hot spot in Fig. 6(*c*) and 7(*c*). At the exit stage of the cutting process, the trailing part of the jet shifts towards the direction of cut. Thus the top of the uncut triangle is hit by the waterjet from both sides which causes the hot spot. The temperature gradient from the entry stage to the exit stage is higher in the case of aluminum compared to that of titanium, which could be due to higher thermal diffusivity of aluminum. Thus, infrared thermography is a useful tool to conduct visualization studies on opaque materials.

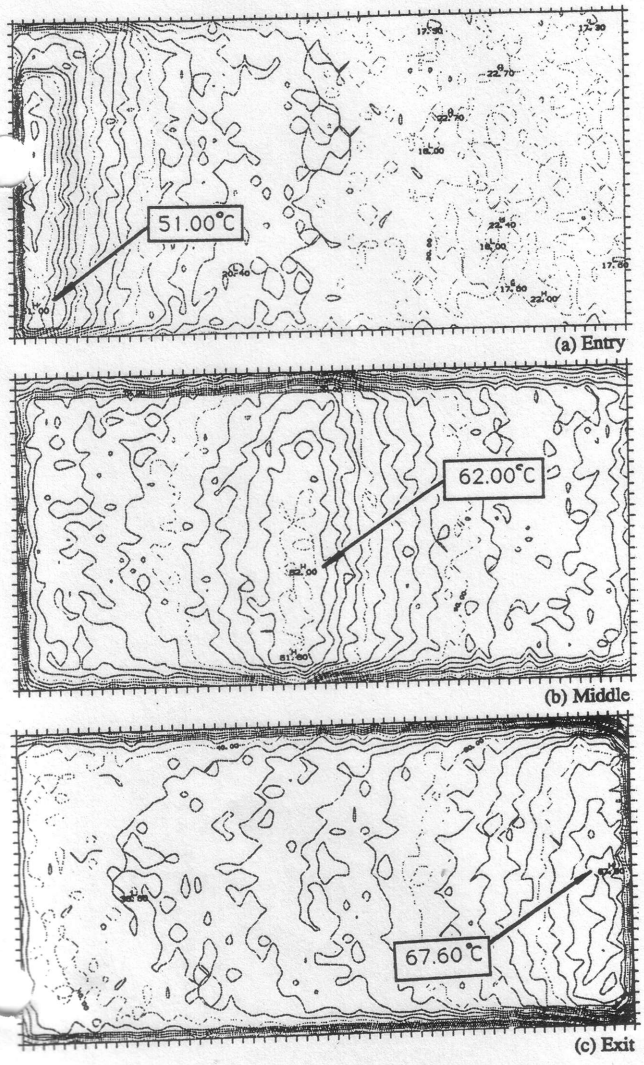

Fig. 6 Visualization of AWJ cutting mechanism in aluminum

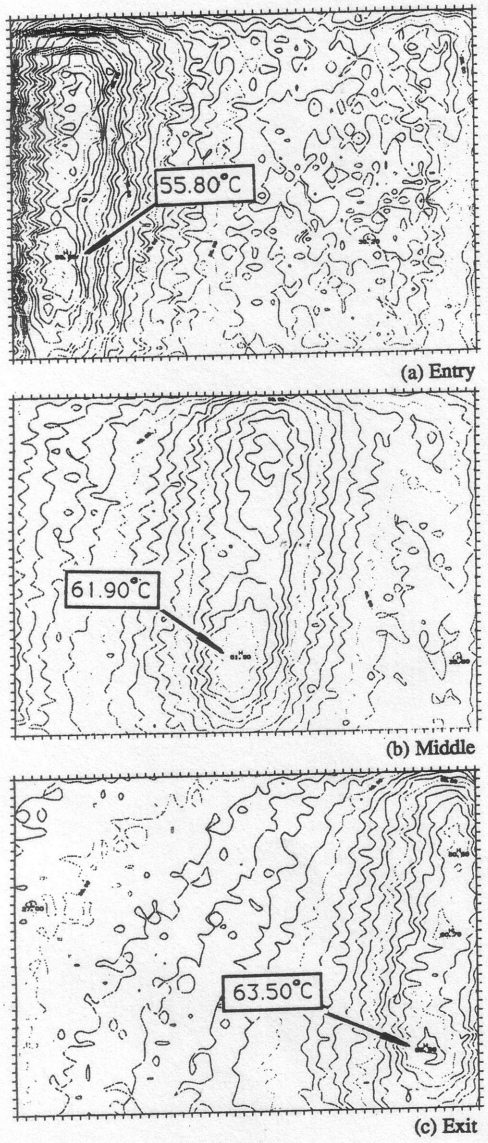

Fig. 7 Visualization of AWJ cutting mechanism in titanium

4.6 Monitoring of Nozzle Wear. The AWJ nozzle focuses a thin stream of high velocity waterjet mixed with abrasives onto the target material. Thus, it is one of the most critical parts of an AWJ cutting system that influences the cutting performance. There has not been any investigation about the distribution of temperature in the abrasive waterjet nozzle to date. The temperature distribution in the nozzle is studied here to develop an alternative method for nozzle wear monitoring through infrared sensing. The sapphire orifice diameter was held constant and the nozzle (mixing tube) was subjected to a gradual wear till the inside diameter increased by 70 percent. The nozzle temperature was measured for three typical nozzle inside diameters. Black enamel of thermal emissivity 0.99 was used to coat the AWJ nozzle to ensure a known, constant emissivity of the nozzle.

Temperature distribution in a partially worn out nozzle is given in Fig. 9(*a*) as a typical example. The relationship between the nozzle peak temperature and its inside diameter is

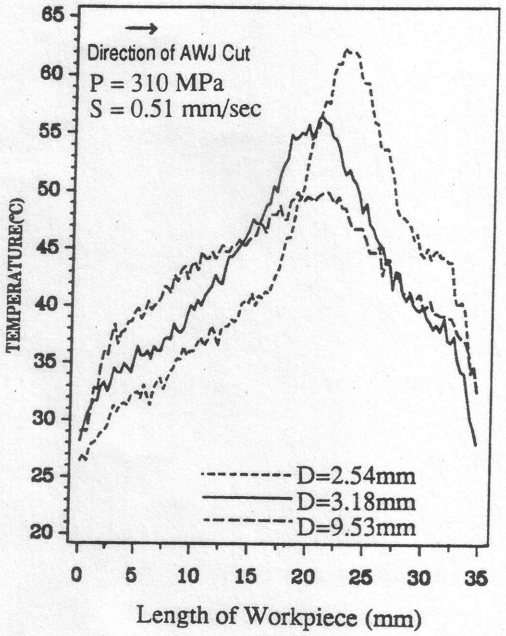

Fig. 8 Linescans with varying distance of cut surface–Phase II (titanium)

given in Fig. 9(*b*). The shift in the position of the peak temperature as nozzle wear progresses is also depicted in Fig. 9(*b*) in which the ratio, L/L_n, is plotted in the y-axis, where, L is the distance between the location of the peak temperature and the top of the nozzle and L_n is the nozzle length. It can noted that as the nozzle inside diameter increases, the peak temperature drops down and its position gets shifted towards the nozzle exit indicating the progress of radial and axial wear. The abrasive entrained waterjet stream passes through the nozzle, causing its erosion leading to a rise in temperature. Initially, the wearing process of the AWJ nozzle is more pronounced at the entry zone (top) of the nozzle, which is characterized by the presence of a hot spot in this zone. However, with continuous usage, the inner walls of the nozzle erode at the entry zone more and the hot spot gets shifted towards the nozzle exit where friction forces are much larger than at the entry zone of the AWJ nozzle. As the nozzle ID increases further, more space is made available for the AWJ stream to flow. This leads to a reduction in the frictional force between the jet and the nozzle walls. As a result the nozzle temperature reduces. The quadratic relationship between the nozzle ID and peak temperature as well as L/L_n ratio indicate that infrared thermography could be a viable alternative technique for AWJ nozzle wear monitoring.

4.7 Comparison of Infrared Data with Thermocouple Data. Temperatures at discrete points on the coated surfaces were measured using thermocouples and the obtained results were compared with the IR thermography results. On the aluminum workpiece, thermocouples were placed at two locations along the central horizontal line of the coated surface. For titanium, thermocouples were placed at two positions along the central vertical line of the coated surface, one in the cutting wear zone and one in the deformation wear zone. Temperature readings of the pixels in the IR images which correspond to the respective locations of the thermocouples were taken for analysis. The time-temperature graphs from the IR images and thermocouples are plotted in Figs. 10(*a*) and 10(*b*) for aluminum and titanium respectively for comparison.

The time-temperature graphs obtained from IR images and thermocouples (for aluminum and titanium) match very closely with each other. From Fig. 10(*a*), it can be seen that the overall workpiece temperature increases as time progresses, indicated by the slightly higher peak temperature towards the end of the cut. The temperature plots in Fig. 10(*b*) show that the lower thermocouple (as well as the corresponding pixel) reaches its peak temperature slightly later than the upper thermocouple (corresponding pixel). This occurrence is due to the deflection of the jet away from the direction of cut (Fig. 10(*b*)). It can also be noted that the peak temperature of the bottom thermocouple is marginally higher than the top one, due to the higher frictional forces in the deformation wear zone.

5 Conclusions

The following conclusions can be drawn from this investigation:

Infrared thermography is found to be an effective technique to monitor the thermal energy distribution in the workpiece. The heat flux at the cut kerf and hence the workpiece temperature increases as water pressure increases. Change in traverse speed has only a marginal effect on the heat flux at the cut kerf and temperature distribution in the workpiece. Peak temperatures occur in the workpiece at regions close to the cutting zone and reduce gradually with increasing distance from the cutting plane.

Infrared imaging can provide more information related to the AWJ cutting mechanisms in terms of jet flow pattern and wear modes for those materials having lower thermal diffusivity. Infrared thermography is found to be a feasible technique for visualization of AWJ cutting mechanisms in opaque materials. Presence of stronger striations (rougher surface) in the kerf wall is characterized by two peak temperatures along the jet

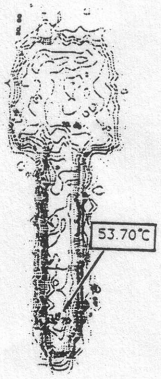

(a) Isotherms

ID=1.40mm

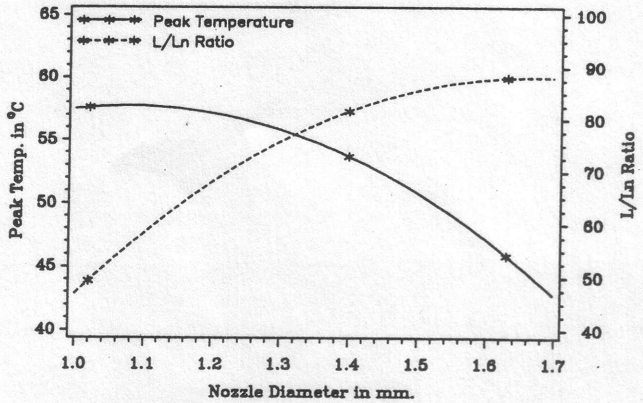

(b) Nozzle Diameter vs. Peak Temperature and L/L_n Ratio.

Fig. 9 Temperature distribution in AWJ nozzle

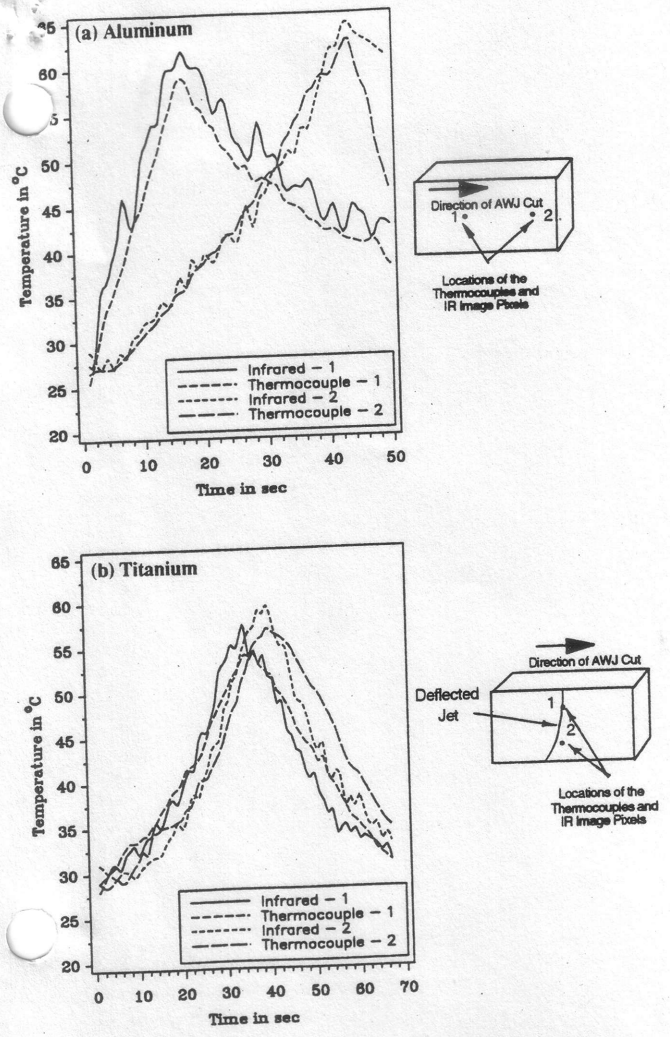

Fig. 10 Comparison of infrared data with thermocouple data

trajectory, whereas weaker striations produce only one peak temperature.

With progressive wear of AWJ nozzle the peak temperature in the nozzle is shifted towards the nozzle exit. Due to reduction in frictional forces between the jet and the nozzle wall, the magnitude of the peak temperature decreases with nozzle wear. Thus, IR thermography could be used as a viable technique for monitoring the axial and radial wear of the AWJ nozzle.

The IR thermography results very closely match with that obtained from the moving line heat source model. Quantitative comparison of IR results with those obtained using thermocouples also shows good agreement. The temperature measurements using IR sensor were found to be repeatable for fixed nozzle position within an accuracy of ±1°C.

Acknowledgements

The authors would like to thank the Center for Robotics and Manufacturing Systems, University of Kentucky, for the financial support in executing this project and Flow International Inc., Kent, Washington, for providing the AWJ cutting system.

References

1 Ohadi, M. M., Ansari, A. L., and Hashish M., 1992, "Thermal Energy Distributions in the Workpiece During Cutting with an Abrasive Waterjet," ASME JOURNAL OF ENGINEERING FOR INDUSTRY, Feb., Vol. 114, pp. 67–73.

2 Ohadi, M. M., and Cheng, K. L., 1993, "Modeling of Temperature Distributions in the Workpiece During Abrasive Waterjet Machining," ASME *Journal of Heat Transfer,* May, Vol. 115, pp. 446–452.

3 Silverman, J., Mooney, J. M., and Shepherd, F. D., 1992, "Infrared Video Cameras," *Scientific American,* March, pp. 78–83.

4 Doong, Ji-Liang, Wu, Ching-Shang, and Hwang, Juin-Ren, 1991, "Infrared Temperature Sensing of Laser Welding," *International Journal of Machine Tools Manufacturing,* Vol. 31, No. 4, pp. 607–616.

5 Lukens, W. E., and Morris, R. A., 1982, "Infrared Temperature Sensing of Cooling Rates for Arc Welding Control," *Welding Journal,* Jan., pp. 27–33.

6 Beardsley, H. E., Zhang, Y. M., and Kovacevic, R., 1993, "Infrared Sensing of Full Penetration State in GTAW," *74th Annual American Welding Society Convention,* April, Houston, TX.

7 Ramsey, Y. P. W., Chyle, J. J., Kuhr, J. N., Myers, P. S., Weiss, M., and Groth, W., 1963, "Infrared Temperature Sensing Systems for Automatic Fusion Welding," *Welding Research Supplement,* Aug., pp. 337–346.

8 Ueda, T., Yamada, K., and Sugita, T., 1992, "Measurement of Grinding Temperature of Ceramics Using Infrared Radiation Pyrometer with Optical Fiber," ASME JOURNAL OF ENGINEERING FOR INDUSTRY, Aug., Vol. 114, pp. 317–322.

9 Hamilton, A., Childs, E., and Kunz, M., 1989, "Infrared Thermographic Evaluation of Fiber-Reinforced Composite Structures with Honeycomb and Closed-Cell Cores," *Proceedings of SME's Conference on Fabricating Composites, IQ89-592,* Oct. 3–5, pp. 1–21.

10 Hashish, M., 1988, "Visualization of the Abrasive Waterjet Cutting Process," *Experimental Mechanics,* June, pp. 159–169.

11 Kovacevic, R., 1988, "Sensor for Detecting the Nozzle Wear in Abrasive Waterjet Cutting Systems," *Invention Disclosure,* Syracuse University, Syracuse, NY, March.

12 Kovacevic, R., 1991, "Development of Opto-electronic Sensor for Monitoring the Abrasive Waterjet Nozzle Wear," ASME Winter Annual Meeting, Symposium on Sensors, Controls and Quality Issues in Manufacturing, Dec. 1–6, Atlanta, GA.

13 Kovacevic, R., and Chen, G., 1989, "A Workpiece Reactive Force as a Parameter for Monitoring the Nozzle Wear in Turning Operation by Abrasive Waterjet," *Proc. of the ASME Winter Annual Meeting, The High Energy Beam Manufacturing Technology Session,* Dec. 14–17, San Francisco, CA.

14 Mohan, R., Kovacevic, R., and Damarla, R., 1994, "Real-time Monitoring of AWJ Nozzle Wear Using Artificial Neural Networks," *NAMRI/SME Transactions, Vol. XXII,* pp. 253–258.

15 Rosenthal, D., 1946, "The Theory of Moving Sources of Heat and its Application to Metal Treatments," *Transactions of the ASME,* Vol. 35, Nov., pp. 849–866.

16 Beck, J. V., and Arnold, K. J., 1977, *Parameter Estimation in Engineering and Science,* Wiley, New York.

17 Rosenthal, D., 1941, "Mathematical Theory of Heat Distribution During Welding and Cutting," *Welding Journal,* May, pp. 220s–234s.

18 Kovacevic, R., Mohan, R., and Zhang, Y. M., 1995, "Cutting Force Dynamics as a Tool for Surface Profile Monitoring in AWJ," ASME JOURNAL OF ENGINEERING FOR INDUSTRY, Aug., Vol. 117 No. 3, pp. 340–350.